

# UNIVERSITÀ DEGLI STUDI DI PADOVA

Dipartimento di Fisica e Astronomia “Galileo Galilei”

Corso di Laurea Magistrale in Fisica

## Phase I of the ANNIE experiment: Data Acquisition system and preliminary data analysis

### RELATORE

Dott. Gianmaria Collazuol

### CANDIDATO:

Tommaso Boschi  
*matr.* 1105506

### CORRELATORI:

Prof. Francesca Di Lodovico (QMUL)

Dr. Benjamin Richards (QMUL)



*Agli amici più grandi.  
A chi ho perso per strada.*



# Overview

This thesis is placed within the context of The Accelerator Neutrino Neutron Interaction Experiment (ANNIE), a water Cherenkov detector built at the Fermi National Accelerator Laboratory. The main aim of ANNIE is to study in depth the nature of neutrino-nucleus interactions by analysing the yield of final state neutrons produced in this kind of interactions. New technologies, such as gadolinium-loaded water and, for the first time, Large Area Picosecond Photodetectors (LAPPDs) will be also employed in future phases of the experiment. The measurement will have relevant implications for next generation Water Cherenkov detectors, in that these techniques may play a significant role in reducing backgrounds in relation to proton decay measurements, supernova neutrino observations and neutrino interaction physics.

This paper deals with the Phase I of the experiment, in which photomultipliers (PMT) are adopted within the tank and the forward Veto and the Muon Range Detector (MRD) are partially being employed. A small container, called Neutron Volume Capture (NVC) is also inside the tank, for preliminary neutron yield studies. The main work of the thesis consists of the development of the CAMAC electronics Data Acquisition system (DAQ); the already existing VME electronics DAQ, for the water PMTs, is also described. Furthermore, early stage data are analysed and studied, and event reconstruction techniques are proposed.

All the described activities were undertaken in the Particle Physics Research Group of the Queen Mary University of London.

This thesis is divided as follows:

**Chapter 1** Neutrino Physics is briefly introduced and the experimental techniques for their detection are listed.

**Chapter 2** The ANNIE Experiment is described.

**Chapter 3** The DAQ system is illustrated, as long as future developments.

**Chapter 4** Data analysis techniques, mainly focused on signal/noise discrimination, are shown. Event reconstruction is also taken in consideration.

**Chapter 5** Measurements and testing the validity of preliminary data analysis undertaken.

**Chapter 6** Conclusion.



# Contents

<b>Overview</b>	<b>iii</b>
<b>1 Introduction</b>	<b>1</b>
1.1 Neutrino Physics . . . . .	3
1.2 Neutrino nucleon interaction . . . . .	3
1.3 Neutrino detection . . . . .	3
1.3.1 Water cherenkov . . . . .	3
1.3.2 Neutron yield . . . . .	4
<b>2 The ANNIE Experiment</b>	<b>5</b>
2.1 Neutrino beam . . . . .	6
2.2 The Hall . . . . .	7
2.2.1 Water tank . . . . .	7
2.2.2 Photodetectors+LAPPDs . . . . .	9
2.2.3 MRD and VETO . . . . .	9
2.3 Expected events . . . . .	10
<b>3 Data Acquisition</b>	<b>11</b>
3.1 Main DAQ Chain and VME Chain . . . . .	12
3.1.1 Hardware . . . . .	12
3.1.2 Software . . . . .	13
3.2 MRD Chain . . . . .	14
3.2.1 Hardware . . . . .	14
3.2.2 Software . . . . .	15
3.3 Future improvement . . . . .	17
<b>4 Analaysis procedures</b>	<b>19</b>
4.1 Inidivual pulse analysis . . . . .	19
4.1.1 Event definition . . . . .	20
4.1.2 Signal and noise discrimination . . . . .	20
<b>5 Measurement</b>	<b>21</b>
5.1 Cosmic background data . . . . .	21
5.2 Threshold dependance . . . . .	21
5.2.1 Voltage . . . . .	21
5.2.2 PMTs fired . . . . .	21
5.2.3 Rejection window . . . . .	21
5.3 Michel decay . . . . .	21
5.4 Neutron yield . . . . .	21
5.5 First MRD data . . . . .	22
<b>6 Conclusions</b>	<b>23</b>
<b>A Booster Neutrino Beam</b>	<b>25</b>
A.1 BNB details . . . . .	25
A.2 Resistive Wall Monitor . . . . .	27

<b>B Employed CAMAC modules</b>	<b>29</b>
B.1 USB Camac Controller . . . . .	29
B.2 TDC . . . . .	29
B.3 ADC . . . . .	29

# Chapter 1

## Introduction

Just copied and pasted random stuff, eventually i'll have to clean this mess. Ignore it for now.

The Standard Model (SM) describes the strong, electromagnetic, and weak interactions of elementary particles in the framework of quantum field theory. It is a gauge theory based on the local symmetry group

$$\mathrm{SU}(3)_C \otimes \mathrm{SU}(2)_L \otimes \mathrm{U}(1)_Y \quad (1.1)$$

where  $C$ ,  $L$  and  $Y$  denote color, left-handed chirality and weak hypercharge, respectively. The gauge group uniquely determines the interactions and the number of vector gauge bosons that correspond to the generators of the group. They are eight massless gluons that mediate strong interactions, corresponding to the eight generators of  $\mathrm{SU}(3)_C$ , and four gauge bosons, of which three are massive ( $W^\pm$  and  $Z$ ) and one is massless, corresponding to the three generators of  $\mathrm{SU}(2)_L$  and one generator of  $\mathrm{U}(1)_Y$ , responsible for electroweak interactions. The electroweak part of the SM, based on the symmetry group  $\mathrm{SU}(2)_L \otimes \mathrm{U}(1)_Y$ , determines the interactions of neutrinos. In the SM, electroweak interactions can be studied separately from strong interactions, because the symmetry under the color group is unbroken and there is no mixing between the  $\mathrm{SU}(3)_C$  and the  $\mathrm{SU}(2)_L \otimes \mathrm{U}(1)_Y$  sectors. Electromagnetic and weak interactions must be treated together because there can be a mixing between the neutral gauge bosons of  $\mathrm{SU}(2)_L$  and  $\mathrm{U}(1)_Y$  [543]. As in all gauge theories, the symmetry group of the SM fixes the interactions, i.e. the number and properties of the vector gauge bosons, with only three independent unknown parameters, the three coupling constants of the  $\mathrm{SU}(3)_C$ ,  $\mathrm{SU}(2)_L$  and  $\mathrm{U}(1)_Y$  groups, all of which must be determined from experiments. On the other hand, the number and properties of scalar bosons and fermions are left unconstrained, except for the fact that they must transform in a definite way under the symmetry group, i.e. they must belong to the representations of the symmetry group, and the fermion representations must lead to the cancellation of quantum anomalies [31, 201, 268, 572, 517]. In the SM, the number of scalar bosons and fermions and their arrangement in the representations of the symmetry group are chosen in a heuristic way. The scalar bosons are chosen in order to implement, in a minimal way, the Higgs mechanism for the generation of masses, whereas the number and properties of fermions are determined by experiments. It is remarkable that all the known elementary fermions can be accommodated in appropriate representations of the symmetry group of the SM with exact cancellation of quantum anomalies. A puzzling feature of Nature is the existence of three generations of fermions with identical properties, except for different masses. This feature is unexplained in the SM. The known elementary fermions are divided in two categories, quarks and leptons [12], according to the scheme 1 st generation quarks: leptons: 2 nd generation 3 rd generation u (up), c (charm), t (top), d (down), s (strange), b (bottom); e (electron neutrino), (muon neutrino), (tau neutrino), e (electron), (muon), (tau). They are distinguished by the fact that quarks participate in all the interactions (strong, electromagnetic, weak, and gravitational), whereas leptons participate in all the interactions except strong interactions. The masses and electric charges of quarks and leptons are given in Tables 3.1 and 3.2. The corresponding antiparticles have the same mass and opposite electric charge. All fundamental fermions have spin 1/2.

A neutrino is a chargless lepton, therefore it is a fermion which interacts only via the weak force.

The predictions of the existence of the  $W$  and  $Z$  bosons, the gluon, the top and charm quarks made the fortune of the Standard Model (SM). Their predicted properties were experimentally confirmed with good precision and the recent discovery of the Higgs Boson [? ] [? ] is the last

crowning achievement of SM.

Despite being the most successful theory of particle physics to date, the Standard Model is actually limited in its approximation to reality, in that some clear evidences cannot be explained. The most outstanding discovery is the neutrino oscillations, which has proved that the neutrinos are not all massless, as it is assumed by theory. Mass terms for the neutrinos can be included in the SM, with the implications of theoretical problems. Likewise, the SM is unable to provide an explanation of the observed asymmetry between matter and anti-matter. It was noted by Sakharov [? ] that a solution to this puzzle would require some form of C and CP violation in the early Universe, along with Baryon number violation and out-of-equilibrium interactions. These facts suggest that the Standard Model is not a complete theory and additional physics Beyond the Standard Model (BSM) is required.

Even though evidence of CP-violation has been found in hadron physics !danielscullyintroduction!, this does not suffice for the asymmetry required to explain cosmological observations. M. Fukugita and T. Yaganida pointed out an elegant mechanism to generate the baryon excess from lepton asymmetries. This process is referred as Leptogenesis and necessitates a Standard Model extension, such as the introduction of right-handed neutrinos, permitting implementation of the see-saw mechanism and providing the neutrinos with mass. On the other hand, the extended model is able to spontaneously generate leptons from the decays of right-handed neutrinos. Eventually, the lepton asymmetry is converted to baryon asymmetry by sphalerons. This process is referred as Leptogenesis and involves Majorana mass terms and the seesaw may transform into the baryon number excess through the unsuppressed baryon number violation of electroweak processes at high temperatures

Once again the discovery of neutrino oscillations could hold the answer since the phenomenon also allows for the possibility of leptonic CP-violation. Various mechanisms have been proposed that would allow CP-violation in the lepton sector to provide the necessary asymmetry in the baryons [5]. Establishing whether or not CP-violation does occur in neutrinos is therefore a priority.

It is clear that the study of neutrinos is of vital importance to the future development of particle physics, in particular through the study of oscillations. However, as will be discussed in Chapter 2, precision measurements of neutrino oscillations are predicated on improving our understanding of neutrino-nucleus interactions.

There are multiple channels through which neutrinos can interact with nuclei and, as described in Chapter 3, many of them are in need of improvements in both our experimental and theoretical understanding. In Chapter 4 one interaction channel, coherent pion production, is identified as being of particular importance to the field, in need of experimental input, and with the potential for significant improvements in the near future. The T2K neutrino oscillation experiment, described in Chapter 5, provided an opportunity to contribute to this field, the results of which are reported in Chapter 6.

The neutrino was postulated first by Wolfgang Pauli in 1930 to explain how beta decay could conserve energy, momentum, and angular momentum (spin). In contrast to Niels Bohr, who proposed a statistical version of the conservation laws to explain the event, Pauli hypothesized an undetected particle that he called a “neutron”, using the same -on ending employed for naming both the proton and the electron. He considered that the new particle was emitted from the nucleus together with the electron or beta particle in the process of beta decay.[8][nb 2]

In Fermi’s theory of beta decay, Chadwick’s large neutral particle could decay to a proton, electron, and the smaller neutral particle (flavored as an electron antineutrino):

Fermi’s paper, written in 1934, unified Pauli’s neutrino with Paul Dirac’s positron and Werner Heisenberg’s neutron–proton model and gave a solid theoretical basis for future experimental work. However, the journal Nature rejected Fermi’s paper, saying that the theory was “too remote from reality”. He submitted the paper to an Italian journal, which accepted it, but the general lack of interest in his theory at that early date caused him to switch to experimental physics.[10]:24[11]

Nevertheless, even in 1934 there were hints that Bohr’s idea — that the energy conservation laws were not followed — was incorrect. At the Solvay conference of 1934, the first measurements of the energy spectra of beta decay were reported, and these spectra were found to impose a strict limit on the energy of electrons from each type of beta decay. Such a limit was not expected if the conservation of energy was not upheld, in which case any amount of energy would be expected to be statistically available in at least a few decays. The natural explanation of the beta decay spectrum as first measured in 1934 was that only a limited (and conserved) amount of energy was available, and a new particle was sometimes taking a varying fraction of this limited energy,

leaving the rest for the beta particle. Pauli made use of the occasion to publicly emphasize that the still-undetected “neutrino” must be an actual particle.

The idea of neutrino was put forward by W. Pauli in 1930. This was a dramatic time in physics. After it was established in the Ellis and Wooster experiment that the average energy of the electrons produced in the beta-decay is significantly smaller than the total released energy, only the existence of neutrino, a neutral particle with a small mass and a large penetration length (much larger than the penetration length of the photon), which is emitted in the  $\beta$ -decay together with the electron, could save the fundamental law of the conservation of energy. At the time when the neutrino hypothesis was proposed the only known elementary particles were electron and proton. In this sense neutrino (more exactly electron neutrino) is one of the “oldest” elementary particles. However, the existence of the neutrino was established only in the middle of the fifties when neutron, muon, pions, kaons,  $\Lambda$  and other strange particles were discovered. We know at present that the twelve fundamental fermions exist in nature: six quarks  $u$ ,  $d$ ,  $c$ ,  $s$ ,  $t$ ,  $b$ , three charged leptons  $e$ ,  $\mu$ ,  $\tau$  and three neutrinos  $\nu_e$ ,  $\nu_\mu$ ,  $\nu_\tau$ . They are grouped in the three families, which differ in masses of particles but have universal electroweak interaction with photons and vector  $W^\pm$ ,  $Z$  bosons. In the Lagrangian of the electroweak interaction, neutrinos enter on the same footings as the quarks and charged leptons. In spite of this similarity of the electroweak interaction neutrinos are special particles.

## 1.1 Neutrino Physics

There are two basic differences between neutrinos and other fundamental fermions.

- At all available at present energies, cross section of the interaction of neutrinos with matter is many order of magnitude smaller than the cross section of the electromagnetic interaction of leptons with matter (via the exchange of the virtual photon). This is connected with the fact that neutrinos interact with matter via the exchange of the heavy virtual  $W^\pm$  and  $Z$  bosons.
- Neutrino masses are many order of the magnitude smaller than the masses of leptons and quarks. Because of the extreme smallness of the neutrino cross section, special methods of the detection of neutrino processes must be developed.

The Physics of neutrino-nucleus interactions is strictly influenced by the complex interplay of multiple particles and current models are limited in their approximation to reality. As more neutrino data become available, lack of knowledge of the fine details of the interactions begins to narrow the reach of future experiments. Under this circumstances, experiments that observe neutrino-nucleus interactions using different techniques are essential to develop more accurate models that allow an era of precision physics in neutrino experiments. A key handle in understanding neutrino-nucleus interaction is the number and type of nucleons ejected from the interaction, which are a valuable constraint on theoretical models.

One example is the first double differential cross section for charged-current quasi-elastic (CCQE) interactions, published by the MiniBooNE experiment [ref]. It has been shown that these and other data are finely described by models including two-body currents, where low-energy neutrinos scatter off correlated pairs of nucleons. A relevant predicted consequence of two-body currents is higher multiplicity of final-state nucleons, indeed.

## 1.2 Neutrino nucleon interaction

### 1.3 Neutrino detection

#### 1.3.1 Water cherenkov

As a charged particle travels, it disrupts the local electromagnetic field in its medium. In particular, the medium becomes electrically polarized by the particle’s electric field. If the particle travels slowly then the disturbance elastically relaxes back to mechanical equilibrium as the particle passes. When the particle is traveling fast enough, however, the limited response speed of the medium means that a disturbance is left in the wake of the particle, and the energy contained in this disturbance radiates as a coherent shockwave.

“Ring-imaging” Cherenkov detectors take advantage of a phenomenon called Cherenkov light. Cherenkov radiation is produced whenever charged particles such as electrons or muons are moving through a given detector medium somewhat faster than the speed of light in that medium. In a Cherenkov detector, a large volume of clear material such as water or ice is surrounded by light-sensitive photomultiplier tubes. A charged lepton produced with sufficient energy and moving through such a detector does travel somewhat faster than the speed of light in the detector medium (although somewhat slower than the speed of light in a vacuum). The charged lepton generates a visible “optical shockwave” of Cherenkov radiation. This radiation is detected by the photomultiplier tubes and shows up as a characteristic ring-like pattern of activity in the array of photomultiplier tubes. As neutrinos can interact with atomic nuclei to produce charged leptons which emit Cherenkov radiation, this pattern can be used to infer direction, energy, and (sometimes) flavor information about incident neutrinos.

### 1.3.2 Neutron yield

## Chapter 2

# The ANNIE Experiment

Final-state neutron abundance from pure neutrino interactions in relation to the energy and the direction of final-state muons with respect to the original neutrino are currently poorly-known and difficult to measure. These combined data can be used to better constrain nuclear models of neutrino interaction physics and are an essential input to Monte Carlo models, used for calculating detection efficiencies, expected background rates, accurate limits, and confidence levels. The count of neutrons can also be used to reject contamination by atmospheric neutrino interactions in proton decay experiments and in a sample of diffuse supernova background neutrinos and may also help to statistically address wrong-sign contamination in oscillation analyses. In addition to helping understand fundamental neutrino-interaction physics, tagging events by the presence and number of final-state neutrons can provide physics analyses with a better handle for signal-background separation and even allow for discrimination between different types of neutrino interactions.



**Figure 2.1:** Logo of the ANNIE experiment.

stream forward Veto and a downstream Muon Range Detector (MRD) are also installed in the hall. The experiment aims to be a test bed for many new technologies, as the gadolinium-doped water and the use of early prototype Large Area Picosecond Photodetectors (LAPPDs). Neutron tagging in Gd-loaded water may play a significant role in reducing backgrounds from atmospheric neutrinos in next generation proton-decay searches using megaton-scale Water Cherenkov detectors, like Hyper-Kamiokande ref. Similar techniques might also be useful in the detection of supernova neutrinos. Accurate determination of neutron tagging efficiencies will require a detailed understanding of the number of neutrons produced by neutrino interactions in water as a function of momentum transferred. To achieve this task, an innovative aspect of the ANNIE design is the use of precision timing to localize interaction vertices in the small fiducial volume of the detector. This experiment will be a first application of these devices demonstrating their feasibility for Water Cherenkov neutrino detectors.

The experiment is planned to proceed in two stages, spread over five years:

**Phase I** a partially-instrumented test-beam run using only Photomultipliers (PMTs) for the purpose of measuring critical neutron backgrounds to the experiment;

**Phase II** a longer run with a more fully-instrumented detector where incremental research and development for the LAPPDs and accompanying fast electronics will be fulfilled, as long as the expansion of the photodetector coverage (both LAPPDs and PMTs) required.

*Year 1* will focus on the R&D, particularly on the development of the Data Acquisition system,

along with the testing in water of the first model of LAPPD. Installation of the first LAPPDs and a significant fraction of the additional PMTs, as well as the calibration system, will take place in *Year 2*. Data-taking would commence in *Year 3* and continue through *Year 5*, with the physics reach of the detector improving as the fraction of LAPPDs increases over time. Publication of derived results would occur by the end of *Year 5*.

This thesis is placed at the beginning of *Year 1*, where testing of the Phase I experimental setup is tested and R%D is undertaken.

## 2.1 Neutrino beam

ANNIE is run on axis from the *Booster Neutrino Beam* (BNB), which deploys 8.89 GeV protons accelerated from the Fermilab booster operating at 15 Hz. The primary beam from the *Linac* uses protons accelerated to 8 GeV kinetic energy by the Fermilab booster. Selected batches containing approximately  $5 \times 10^{12}$  protons are extracted and bent toward a beryllium target via dipole magnets. Each spill is composed of 81 bunches of protons, approximately 6 ns wide each and 19 ns apart, for a total spill duration of 1.6  $\mu$ s. Beam proton trajectories and positions are monitored on a pulse-by-pulse basis. Upstream of the target, the primary proton beam is monitored on a pulse-by-pulse basis using four systems: two toroids measuring its intensity (protons-per-pulse), beam position monitors (BPM) and a multiwire chamber determining the beam width and position, and a resistive wall monitor (RWM) measuring both the time and intensity of the beam spills. A logic signal is also generated by the last device for every intensity peak. It is employed to trigger the experiment in correspondence of each spill. The BNB is dealt in detail in the appendix B.

Hadronic interactions of the protons with the target material produce a beam of secondary mesons, mostly pions and kaons. A magnetic focusing horn, shown in Fig. 2.2, surrounds the beryllium target, bending and sign-selecting the secondary particles emitted along the direction pointing to the hall. The focusing is produced by the toroidal magnetic field present in the air volume between the horn's two coaxial conductors made of aluminum alloy. The beam of focused, secondary mesons emerging from the target/horn region is further collimated, via passive shielding, and allowed to decay into neutrinos in a cylindrical decay region filled with air at atmospheric pressure, 50 m long and 90 cm in radius.

The polarity of the horn current flow can be (and has been) switched, in order to focus negatively charged mesons, and therefore produce an antineutrino instead of a neutrino beam. The  $\pi^\pm$  mesons have a mass of 139.6 MeV and a mean lifetime of  $2.6 \times 10^{-8}$  s. The primary decay mode of a pion, with a branching fraction of 99.9877 %, is a leptonic decay into a muon and a muon neutrino:

$$\pi^+ \rightarrow \mu^+ \nu_\mu \quad (2.1)$$

$$\pi^- \rightarrow \mu^- \bar{\nu}_\mu \quad (2.2)$$

The second most common decay mode of a pion, with a branching fraction of 0.0123 %, is also a leptonic decay into an electron and the corresponding electron antineutrino:

$$\pi^+ \rightarrow e^+ \nu_e \quad (2.3)$$

$$\pi^- \rightarrow e^- \bar{\nu}_e \quad (2.4)$$

In spite of the considerable differences in the space momentum, the suppression of the electronic decay mode with respect to the muonic one is a well known effect, called *helicity suppression*: due to the great mass of the muon ( $m_\mu = 105.658$  MeV) compared to the electron ( $m_e = 0.510$  MeV), the helicity-chirality correspondence is stronger for the latter. Given that the  $\pi$  mesons are spinless, neutrinos are left-handed, and antineutrinos are right-handed, the muonic channel is preferred because of spin and linear momentum preservation. The suppression of the electronic decay mode with respect to the muonic one is given approximately within radiative corrections by the ratio:

$$R_\pi = \left( \frac{m_e}{m_\mu} \right)^2 \left( \frac{m_\pi^2 - m_e^2}{m_\pi^2 - m_\mu^2} \right) = 1.283 \times 10^{-4} \quad (2.5)$$

Have to add something about muon decay here. A beam absorber located at the end of the decay region stops the hadronic and muonic component of the beam, and only an almost pure neutrino beam pointing towards the detector remains.

**From SciBooNE - charged current etc.** Neutrino flux predictions are the same produced by the SciBooNE collaboration, obtained via a GEANT4-based beam Monte Carlo simulation. The same simulation code developed by the MiniBooNE Collaboration is used [24], where a realistic description of the geometry and materials present in the BNB target hall and decay region is used. Primary protons are generated according to the expected beam optics properties upstream of the target. The interactions of primary protons with the beryllium target are simulated according to state-of-the-art hadron interaction data. Of particular importance for this analysis is a  $\pi^+$  production in proton-beryllium interactions, which uses experimental input from the HARP [25] and BNL E910 [26] experiments. Production of secondary protons, neutrons, charged pions, and charged and neutral kaons is taken into account, and elastic and quasielastic scattering of protons in the target are also simulated. Particles emanating from the primary proton-beryllium interaction in the target are then propagated within the GEANT4 framework, which accounts for all relevant physics processes. Given the importance of the target (beryllium and aluminum) hadronic reactions, these are described by custom models, while other hadronic processes and all electromagnetic processes (energy loss, multiple scattering, effect of horn magnetic field, etc.) are described according to default GEANT4 physics lists.

A second, FORTRAN-based Monte Carlo code is responsible for generating the neutrino kinematics distributions from meson and muon decays, and for obtaining the final neutrino fluxes extrapolated to the detector hall with negligible beam Monte Carlo statistical errors. Once produced by the simulation, neutrinos are extrapolated along straight lines toward the detector and all neutrinos whose traces cross any part of the active volume are considered for the flux predictions. Based on accurate survey data, the distance between the center of the beryllium target and the center of the SciBar detector is taken to be 99.9 m, with the detector located on beam axis within a tolerance of a few centimeters.

The neutrino flux prediction at the detector location and as a function of neutrino energy is shown in Fig. 2.3. A total neutrino flux per proton on target of  $2.2 \times 10^{-8} \text{ cm}^{-2}$  is expected at the hall location and in neutrino running mode (positive horn polarity), with a mean neutrino energy of 0.7 GeV. The flux is dominated by muon neutrinos (93% of total), with small contributions from muon antineutrinos (6.4%), and electron neutrinos and antineutrinos (0.6% in total). For the neutrino flux predictions, no information from BNB (SciBooNE or MiniBooNE) neutrino data was used as experimental input.

## 2.2 The Hall

The experiment is set up in the former location of the SciBooNE experiment refagain?, 8 m below the surface and the 100 m from the BNBtarget. Already existing instrumentation in the hall is borrowed by the ANNIE experiment.

### 2.2.1 Water tank

tank = PMTs, water, future LAPPDs and Gd (NCV). Very messy now

The main component of the experiment is the water tank, installed in the SciBooNE hall at Fermilab. Incom Inc, the company selected to commercialize the LAPPD photodetectors, has provided a quote to the ANNIE collaboration committing to produce 20 detectors This is already price-competitive per unit area with equivalent technologies offering similar capabilities (a single LAPPD covers 16 times the area of a 10k 2" Photonis Planacon MCP-PMT and 64 times that

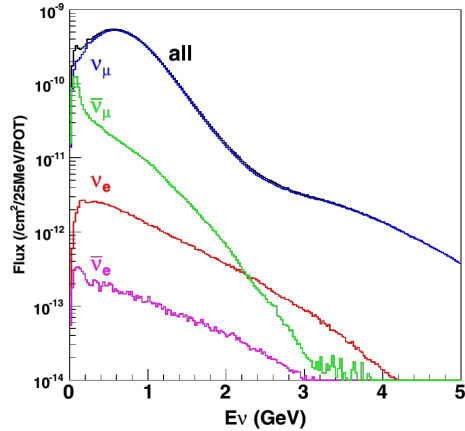


**Figure 2.3:** Neutrino flux predictions from the GEANT4/FORTRAN simulation.

of an 8k Hamamatsu 1 inch tube). These early LAPPDs will be produced in small batches over a period of several years, with the first two LAPPDs arriving no later than September 2016 and 5-8 more tiles in September 2017. Specifications of the LAPPDs are derived from prior tests: time resolutions below 100 psec, spatial resolutions below 1 cm, and gains above  $1 \times 10^7$  [21], as well as 20 % quantum efficiency photocathodes and good gain uniformity [32]. The LAPPD purchase by the ANNIE collaboration represents a technology investment that will pay out past its experimental lifecycle. Their use in ANNIE provides an essential proof-of-principle demonstration of the technology and LAPPDs purchased through ISU can be made available for future HEP efforts after ANNIE. Application-specific detector development work necessary to deploy LAPPDs for use in water is also required. The devices need to be characterized and—along with their high voltage connections and front-end readout boards—must be mounted and placed in the water volume. Water submersion tests (including tests using the full ANNIE water volume) will proceed first using several 6 cm photosensors provided by ANL, built using a similar design and process to the Incom LAPPDs. 14ANL will also design and provide an 8" x 8" structure on which to mount the 6 cm tiles, compatible with the waterproof housing for full-size detectors. The additional development of electronics to read out the LAPPDs and its impact on the overall DAQ system is described in Sec 4.7. One or more publications on the novel instrumentation of ANNIE are planned. In order to guarantee physics results from this effort independently of the status of LAPPD production, an alternative choice for light detectors will be developed in parallel. The optimal choice at this stage would appear to be the Hamamatsu H11934-200 ultra bialkali 1-inch PMTs. With a quantum efficiency of 43 %, comparable photon collection efficiencies to LAPPDs can be achieved with less spatial coverage. The combination of 270 psec time resolutions and fine granularity of these detectors provides capabilities comparable to those discussed in Sec 3.4 (see Fig 6). A quote for 600 of these tubes has been obtained from Hamamatsu and is comparable in cost with the equivalent area x coverage scenario proposed with LAPPDs. It would rely on the same electronics, and mixed 1-inch and LAPPD scenarios are also possible. The group at Lawrence Berkeley National Laboratory (LBNL), led by PI Orebi Gann, is already working with these tubes in a bench-top scale water-based liquid scintillator setup aimed at demonstrating ring imaging for high-energy events in this target medium, leveraging funding by the LBNL LDRD program.

Photodetection in ANNIE Run I will be provided by of 60 8 Hamamatsu PMTs, from a stock of Super-K spares

**Improve Gd section.** Gadolinium in water (NCV) EDGAS and other experiments. The Super-Kamiokande (SK) [1] is the largest light water Cherenkov detector that has been successfully observing solar, atmospheric and accelerator neutrinos. Recently the addition of 0.2 % of a water soluble gadolinium (Gd) compound to SK has been proposed [2]. This modification can greatly improve the detection sensitivity of anti-electron neutrinos. The inverse beta interaction in the water, emits a positron and a neutron. The positron, radiating Cherenkov photons, is immediately detected. The neutron is quickly thermalized in the water, and is then captured by Gd with a probability of 90 %. Upon capturing a neutron the Gd emits 3-4 gamma rays having a total energy of about 8 MeV. The time and spatial correlation of the positron and neutron capture events (20 us and 4 cm) can significantly reduce the backgrounds, and hence enhance the nu e signal events.

## 2.2.2 Photodetectors+LAPPDs

Photomultiplier tubes As noted earlier, ANNIE Phase II will achieve the necessary coverage to detected neutron capture in Gd-loaded water using by: (1) utilizing twenty in-hand 11-inch L PMTs (refurbished proto-types developed under R&D grants from the NSF and DNN), (2) purchasing 50 new HQE 10-inch Hamamatsu PMTs (45+5 spares), and (3) re-using the 8-inch Hamamatsu PMTs refurbished by UC Irvine for ANNIE Phase I. We request funds to purchase

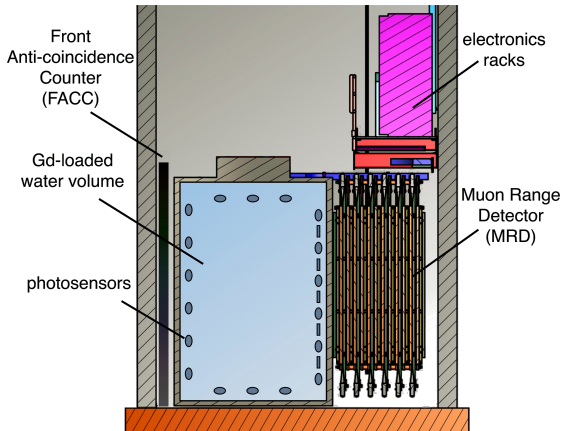


**Figure 2.4:** Schematic of the experimental hall.

the HQE 10-inch PMTs, but with a reserve option to purchase 140 new 8-inch normal QE PMTs (the higher-cost, higher-channel-density option). More detailed simulations will enable a final decision by the collaboration before procurement of the conventional PMT system. Calibration, testing and installation of these PMTs will be carried out by UC Davies and/or UC Irvine.

List of pmts employed??

Talk about LAPPDs

### 2.2.3 Muon Range Detector+Veto

**mostly ok, I guess I have every information.**

A Forward Anti-Coincidence Counter (FACC) consisting of two layers of overlapping muon paddles detects charged particles produced in the dirt upstream of the hall. This allows the rejection of events in the tank unrelated to the beam.

An iron-scintillator sandwich muon range detector (MRD), already in the experimental hall, will be used to range out and fit the direction of daughter muons from neutrino interactions in the water target. Neutrino interactions in the water target will produce light with no signal in the FACC and those that are muon neutrino charged current will likely produce a muon going through the MRD.

The role of the Muon Range Detector is to confine the muons produced in charge-current quasi-elastic (CCQE) interactions, which is the dominant process in SciBooNE. By confining the muon its energy can be reconstructed thus giving a handle on the neutrino energy. The MRD consists of 13 alternating horizontal and vertical scintillator planes, each separated by a 5 cm iron sheet. This results in 60 cm of absorber equivalent to stopping a 1 GeV muon. The first plane is directly downstream of the EC allowing for better track matching and energy reconstruction of p衰0 decay photons that escape the EC. Three planes are required to be hit for a track to be reconstructed in the MRD, equivalent to approximately a 180 MeV muon. The total mass of the detector is 60 tonnes, of which approximately 48 tonnes is absorber. Planes can be moved forward or backward via the use of winches attached to the side of the support frame. There are 362 channels in total; 182 horizontal, 180 vertical. Each channel is 20 cm wide and either 155 cm (horizontal) or 138 cm (vertical) long. Planes have active areas of 310per260 cm<sup>2</sup> (horizontal) and 300per276 cm<sup>2</sup> (vertical). Of these 362 channels 5 different photomultiplier tubes (PMTs) are used. The horizontal planes consist of 14 stage EMI 9954KB PMTs from the KTeV experiment, as well as EMI 9839b and 9939b PMTs. The vertical planes consist of 10 stage Hamamatsu 2154-05 PMTs from the NuTeV experiment and RCA 6392A PMTs. The electronics consist of LeCroy 4300B ADCs, LeCroy 3377 TDCs and the LeCroy 1440 high voltage system.

ANNIE makes use of an existing Muon Range Detector (MRD) that remains mostly intact in the experimental hall. The MRD is a steel and plastic scintillator sandwich detector, designed to range GeV-scale muons and provide directional information. The electronics and high voltage (both for the MRD and photosensors in the water volume) will be provided by Fermilab PREP for the duration of the experiment. Several layers of muon paddles and PMTs are absent; Fermilab has agreed to provide materials and instructional support to the ANNIE collaboration to replace the missing paddles.

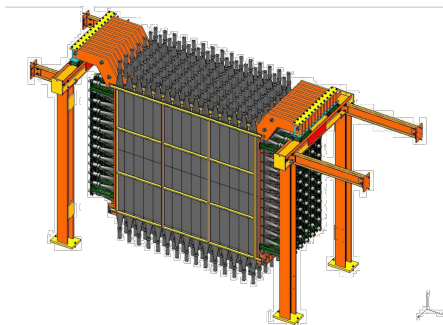


**Figure 2.5:** Drawing of the MRD.

A fraction of the MRD will be made operational for Phase I of ANNIE in early fall. Refurbishment activities by UC Davies will be scheduled after this phase is completed taking so that the detector system is fully operational in time for ANNIE first physics runs. ANNIE will rely on a Forward Anti-Coincidence Counter (FACC) consisting of 2 layers of overlapping muon paddles to reject charged particles produced in dirt, upstream of the hall. Fermilab provided a stock of 60 muon paddles taken from the CDF experiment, from which a subset of 26 paddles were systematically tested and selected. These paddles have already been

attached to the wall by students from UC Davis with the help of Fermilab technicians, using standard 80/20 aluminum extrusions and brackets, arranged in two staggered layers of 13 paddles

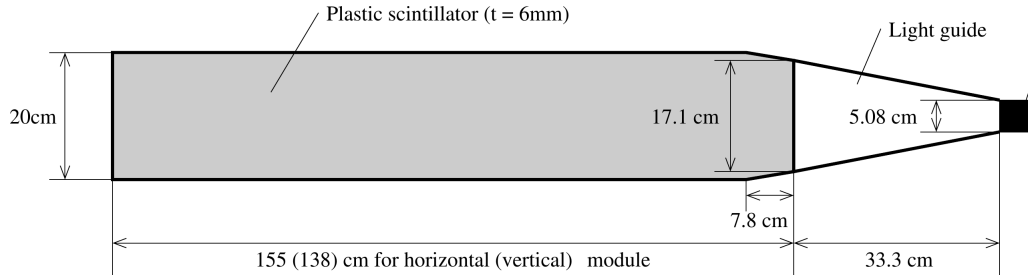


**Figure 2.6:** Paddle used for the MRD.

each.

### 2.3 Expected events

**Odd section.** A beam event should produce a muon in the tank, so the Veto shouldn't fire, some Cherenkov light could be captured by the PMTs and a clear signal is found in the MRD.

## Chapter 3

# Data Acquisition system

Modern high energy Physics experiment's require automated procedures to collect data from detectors and save them in long term storage for ensuing analysis. These routines are gathered in automated system called Data Acquisition system (DAQ), which typically includes three fundamental components:

1. sensors, to convert physical parameters to electrical signals;
2. signal conditioning circuitry, to convert sensor signals into a form that can be converted to digital values.
3. conversion from analog signals to digital values and subsequent storage.

The last step is vital in that it allows data manipulation and analysis by a computer.

As far as ANNIE is concerned, the first requirement has already been discussed in section ref: the experiment has multiple simultaneous data sources, i.e. the forward Veto, water PMTs and the MRD, as well as a blend of front-end electronics technologies (VME, CAMAC and custom FADCs) for ADC/TDC and waveform digitisation. Considering this variety of devices, the whole system has also some requirements to achieve:

- stability, on long acquisition runs;
- control all the aspect of the experiment;
- real time online monitoring;
- direct and remote user control.

Provided a solid electronic system, these tasks are thoroughly accomplished on the software's side, since the system is based upon the *ToolDAQ Framework*<sup>1</sup>, developed by Dr Benjamin Richards [ref] for the Hyper Kamiokande collaboration (HK). The HK group has used this opportunity to undertake R&D and testing of DAQ software and tools for future use in the HK experiment. ANNIE experiment has allowed extensive testing of the flexibility of the software and all the above features to take place within a single deployment.

ToolDAQ is designed to incorporate the best features of other frameworks along with:

- being very easy and fast to develop DAQ implementations in a very modular way;
- Dynamic Service Discovery and Publishing;
- scalable network infrastructure (provided by ZeroMQ) to allow its use on large scale experiments.

---

<sup>1</sup>ToolDAQ is open source and available on GitHub [repo].

The main executable relies on user-defined modular classes, called *Tools*, which present three chief functions, *Initialise*, *Execute*, and *Finalise*. The Tools can be daisy-chained to a *ToolChain* and then handled sequentially by the process whenever one of those functions is called. A ToolChain also manages the more complicated aspects of the DAQ system, like the remote control, the service discovery, and the status of the contained Tools. Parameters, data and other variables are passed between Tools by an editable shared data class. Each tool is allowed to read, update, and modify it, due to it is owned by the ToolChain. The bare structure is sketched in Fig. 3.1.

In the following sections, the whole DAQ structure is analysed as it currently is. It is composed of three parallel ToolChains: the Main DAQ Chain, the VME Chain, and the CAMAC/MRD Chain. The latter hasn't been implemented in the Main DAQ system yet, which is composed by the first two Chains only. At the moment the MRD Chain/DAQ is employed as a standalone DAQ, working in parallel with the Main DAQ, on a different machine with resulting difficulties. Future integration of the two DAQ in the same machine are also discussed.

## 3.1 Main DAQ Chain and VME Chain

### 3.1.1 Hardware

The primary readout for ANNIE Phase I is provided by a VME-based system developed for the KOTO experiment<sup>2</sup> by University of Chicago. The *VMEbus* is a computer architecture, where "VME" stands for VERSA Module Eurocard. It was originally developed by the Motorola, Mostek, and Signetics group, but later was widely used for many applications and eventually standardised by the IEC as ANSI/IEEE 1014-1987. This bus is widely used in High Energy Physics due to the fact that it is of public domain and its data transfer speed is quite fast: for instance the latest manifestation, the VME320/2eSST protocol, can double the theoretical bandwidth of VME to 320MB/s. cite[<http://www.vita.com/VME320-2eSST-Protocol>].

The crates are governed by a VME-based CPU board which runs Internet Rack Monitor software. This latest version runs on the MVME162-22 cpu board with MC68040 cpu, 4MB dynamic ram, 0.5MB static ram, 1MB flash memory, ethernet interface, and support for up to four IndustryPack daughter boards. The latter allows connection to I/O signals via ribbon cables to digital and analog interface boards mounted inside the IRM chassis. The ethernet interface allows network connection and supports widely-used Internet protocols that allow data request and setting access as well as alarm reporting, all based upon the UDP (User Datagram Protocol) transport layer.

The system consists of two types of VME module:

- 4-channel 500 MHz sampling pipeline 14 bit custom FADC cards, which primarily record the traces from the PMTs in the ANNIE water volume.
- Master Trigger (MT) cards which distribute the 125 MHz clock, synchronises the FADC cards, provides the trigger, and provides a busy signal.

The leading edge of photomultiplier signal is too fast for an 8-ns sampling. To avoid dead time and allow the 500 MHz sampling, the output signals from the detectors are stored in 8000 samples pipelines inside Field Programmable Gate Arrays (FPGAs) until a trigger decision is made. The three levels trigger system uses the waveform information with increased sophistication at each level. Each MT card can address 8 FADC cards, but can be daisy-chained or arranged hierarchically to address more total cards. Given the 16 FADC cards of the ANNIE readout, 3 MT cards are used: one Level-0 card distributes the clock between two Level-1 MT cards, each addressing 8 FADCs.

---

<sup>2</sup>The KOTO experiment at J-PARC, Japan, aims at observing the rare kaon decay  $K_L \rightarrow \pi^0 \bar{\nu}\nu$  to search for new physics beyond the standard model that breaks the CP symmetry. The experiment, with a new beam line and new detector components, is underway and the first run was performed in May 2013.

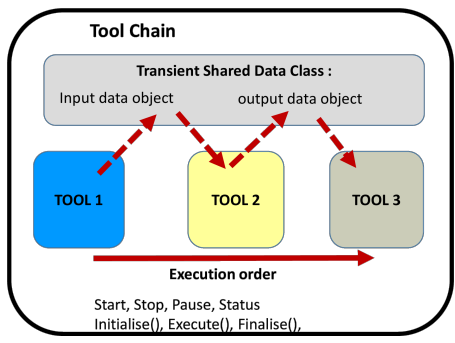


Figure 3.1: Schematic of a ToolChain.

The Muon Range Detector and the Forward Veto nominally rely on the same FADC system as the PMTs in the water volume for the first runs. The signals coming from the paddles are combined through an analog OR and sent to a few spare FADC channels on the KOTO boards.

The instrumenting the ANNIE water volume are operated at positive HV with a single cable for both power and signal. Splitter boxes will be necessary to separate the PMT signal and the HV. ANNIE uses a CAEN system to provide the positive and negative high voltages necessary for operation. A stock of 6 A734P cards suffices to power the 62 large PMTs in the water volume and the 26 positive HV PMTs in the MRD. 26 negative HV channels are also needed for the Forward Veto and another 52 channels to power at least two layers of the MRD.

For storage limitations, a downsampling to 125 MHz was established. The resolution of 8 ns suffices the needs of the R&D stage of Phase I. An 80  $\mu$ s long time window was chosen, therefore with this resolution, four data sets can be held in the 40000 samples buffer. Each set corresponds to a spill from the beam.

### 3.1.2 Software

The data from the water PMTs and the logical sum from the Veto and MRD are acquired by the Main DAQ, which hinges upon two strictly complementary ToolChains: the Main Chain and the VME Chain. The Main Chain is the primary ToolChain of the DAQ system, which communicates with the other two processes.

The Chain's tools are depicted in Fig. 3.2 and they are the following:

Main DAQ	VME
Input variables	
PostSQL	VME Trigger Send
Trigger	Board Reader
Network Receive Data	Network Send Data
Monitor	
Data Recorder	

The *Input variables* tool loads some initialisation parameters and the specification of the current *run*, i.e. data taking session. Three typologies of run are available and are sent to the VME CPU: a test run, an LED run for PMTs calibration, a pedestal run, and a beam run. The triggering of the digitisers is influenced by changing the kind of the run. For instance, a beam run is triggered by the RWM, while an LED run is triggered by the LED pulser. The *PostSQL* tool updates an SQL database of the DAQ, where all the information about the run, such as the number of events, the start and the stop time, and others, are saved. Proper data logging is a fundamental step, especially for Phase I: both the experiment and the DAQ are frequently revised and **knowing which run is which is pretty cool**. *Trigger* tool blocks the Chain, awaiting and sending a trigger query from the VME. When the VME replies, the Chain is run back again. As explained, four 10000samples data sets are collected from the VME cards, which equates to four consecutive spills from the beam. The *Network receive data* tool handles the data transfer via ZeroMQ messaging<sup>3</sup> between the main chain and the VME one. Like most of the HEP experiments, even ANNIE requires real-time monitoring so as to check whether the DAQ system works flawlessly. This is achieved by the *Monitor* tool, which updates a dedicated web-page with random plots of data collected.

On the VME electronics side, the Chain communicates with the VME CPU retrieving all the informations about the cards and the trigger. The *Trigger Sender* tool check the status of the VME controller. If the ADC are triggered, a trigger message is sent to the Main Chain. The data are dumped from the FPGA's buffer by the *Board Reader* tool and are sent to the Main Chain via ZeroMQ messaging over TCP.

The last tool of the Main Chain, *Data recorder*, saves data into the following ROOT tree structure:

<sup>3</sup>ZeroMQ is a high-performance asynchronous messaging library, aimed at use in distributed applications. The API provides *sockets*, each of which can represent a many-to-many connection between endpoints, operating with a message-wise granularity. ZeroMQ is developed by a large community of contributors and distributed under the LGPL license. <http://zeromq.org/>

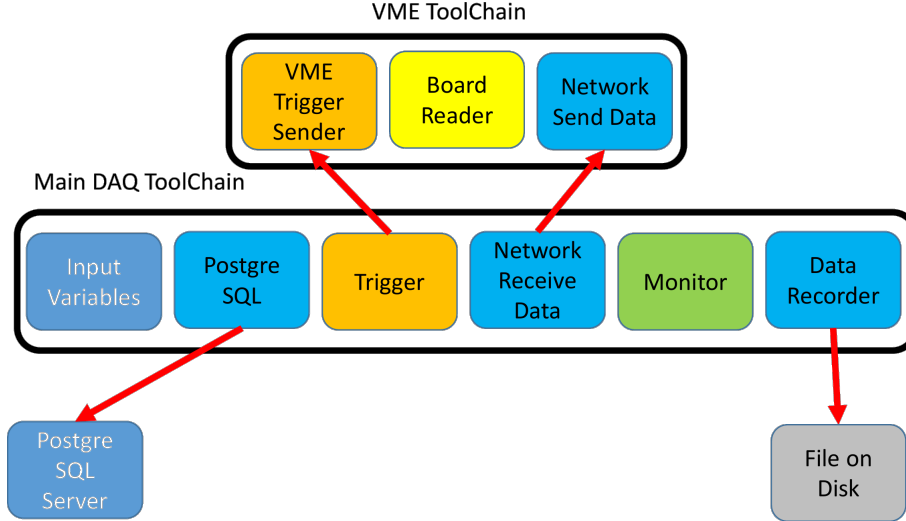


**Figure 3.2:** ANNIE's current main DAQ makes use of two parallel tool chains.

**LastSync** : time of data acquisition;  
**SequenceID** : incrementale number;  
**StartTime** : same as lastsync;  
**CardID** : number of ADC card;  
**Channels** : channel of ADC card;  
**PMTID** : global identifier of PMT (labelled from 1 to 60);  
**BufferSize** : size of the buffer per channel;  
**FullBufferSize** : size of the buffer per card;  
**Data** : array holding the full buffer.

Each entry corresponds to an acquisition of the full buffer from the cards saved in a 40000 long float array, i.e. the digitised time profile of four consecutive  $80 \mu\text{s}$  data set. The ROOT files are then post processed: the buffer is split and an entry is created for each beam event and the precise time stamp is reconstructed.

Have to talk about output format too.

Provided that the spill's frequency is  $\sim 15$  Hz and four spills are acquired, the buffer takes around a quarter of a second to fill. The longest portion of the chain to execute is the disk saving and it is meant to be done between pulse trains, so as to minimse the number of spill lost. A whole execution of the chain lasts nearly a second, slightly less than the pulse train frequency.

Talk about speed of software.

## 3.2 MRD Chain

### 3.2.1 Hardware

As explained in Sec. 3.2[edit to section of VME], the signal from the FACC and two layers of the MRD are logically summed and read by the VME digitisers. The PMTs of these two detectors are supposed to be read individually by both Time-to-Digital Converters (TDC) and ADCs in future stages of the experiment and for this purpose a third ToolChain has been developed to collect data from both the VETO and the MRD's second and third layers (see section ref). CAMAC electronic modules are employed for these two detectors: LeCroy 3377 modules for the time digitisation, while LeCroy 4300B for analog conversion.

*Computer-Aided Measurement And Control* (CAMAC) is a bus and modular-crate electronic standard for data acquisition and control used mainly in nuclear and particle physics experiments

and in industry. The bus allows data exchange between plug-in modules and a crate controller, which then interfaces to a CPU or to a VME-CAMAC interface. The standard was originally defined by the ESONE Committee as standard EUR-4100 in 1972.

The LeCroy Model 3377 is a 32-channel time-to-digital converter (TDC) and optimised with a low conversion time and a high speed readout of 100 ns/word. With 10-bit words, the longest time window achievable is 4088.0 ns, using a resolution of 4.0 ns. A delayed signal from the RWM acts as a “common start” for the TDC cards and each internal counter is individually stopped by hit signals. The channels are fed with the discriminated PMT signals of the VETO and of the second and the third layer of the MRD.

The LeCroy Model 4300B FERA contains 16 independent 11bit charge-to-digital converters. An 8-bit register and a memory containing the individual pedestal values to be subtracted from each ADC are also available. These converters haven’t been installed in the electronic chain yet. Nevertheless the software interface has been developed anyway.

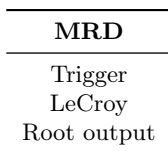
All the cards are addressed via the Weiner CCUSB controller module. The CCUSB is a full-featured CAMAC Crate controller with integrated high speed USB-2 interface. For fast data acquisition applications the CCUSB has a built-in command list sequencer, called *command stack* with data buffering in a 22kB size FIFO. A XILINX Spartan 3 family FPGA performs all CCUSB logic and functions. [More on this?](#)

### 3.2.2 Software

The thesis’s work is mainly focused on the development of a dedicated data acquisition system for the CAMAC electronics of the experiment. A separate MRD DAQ has been created from scratch within the ToolDAQ Framework in order to acquire the MRD and the forward Veto data. These two detectors rely on the CAMAC electronics for front-end read out of the PMTs signals and the USB controller vendor provides a C++ class to interface the controller with the computer.

Some C++ classes were developed with the purpose of handling more easily the modules. A base class takes care of opening the USB connection for the CCUSB controller and storing information on the cards, such as the Slot number. It also allows the configuration of the command stack, i.e. the CAMAC command sequencer. Two derived classes implement wrapper functions to deliver CAMAC commands via the NAF addressing<sup>4</sup>.

The MRD’s ToolChain employs the CAMAC classes to interface with the controller and the cards. As illustrated in Fig. 3.2, the Tools contained in the Chain are: [picure of mrd chain alone](#).



The *Trigger* tool reads the FIFO of a specified card: if it is not empty, then all cards presenting data are read and other tools are executed. Currently, a hit signal is generated in each TDCs by delaying the common start signal of  $\sim 1 \mu\text{s}$ , such that the FIFOs are never empty in coincidence with the beam’s spills. Three triggering behaviours are supported: external trigger, software trigger with random card access, and software trigger with card test function.

The *LeCroy* tool is meant to work for both the TDCs and ADCs cards. If only either TDCs or ADCs are employed, then only one tool should be added in the *ToolChain*. Otherwise, if both are used, then two *LeCroy* tools are required. Given that the ADCs haven’t been installed in the crates yet, only one tool is needed for the TDCs. Nevertheless the charge converters have been tested, as well.

The last tool fills a ROOT tree and save it to file. The tree has the following branches:

---

<sup>4</sup>Module addressing is achieved knowing the slot Number, the subAddress, and the Function code.

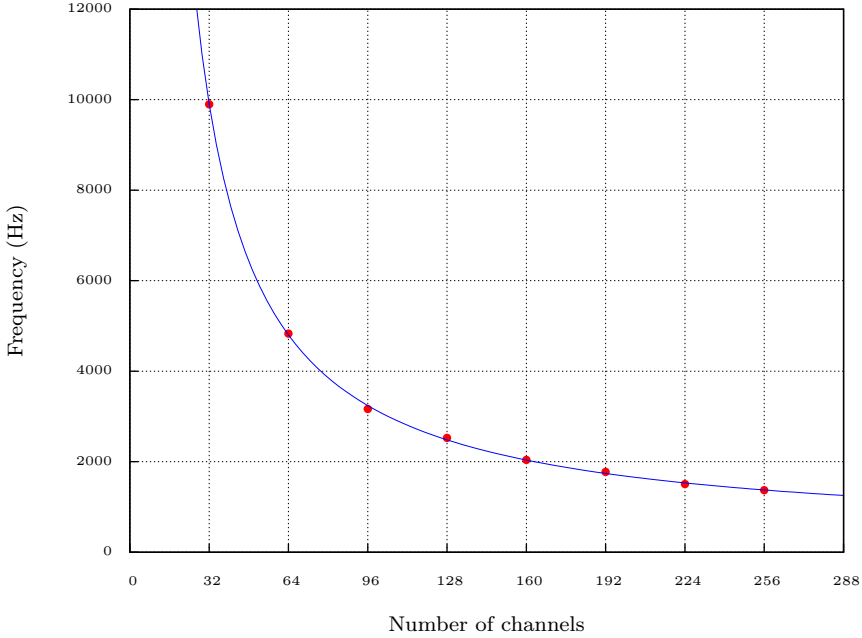


**Figure 3.3:** DAQ frequency reading TDCs with all channels fired, but 1.6% time occupancy.

**Trigger** : incremental number of the trigger;

**OutNumber** : number of channels read;

**Type** : string telling whether the data refer to TDC or to ADC;

**Value** : actual value retrieved from the card.

**Slot** : slot number of the card;

**Channel** : channel of the card from which the value was retrieved;

**TimeStamp** : UNIX time stamp of the entry, since epoch, in ms.

The MRD Chain runs in a different PC than the Main DAQ and the ToolChain is executed at a different speed, for it is a standalone process. For this reason, a method has been realised to correlate the events between the two DAQs. Timestamps were designated for this fundamental task: both DAQs assign UNIX time to each event, since the clocks are synchronised to the same NTP server, which uses GPS time sources. With the help of the Fermilab spill database [ref here], the events from the two DAQs can be related to each other.

This method is effective as long as the frequency of the chain execution is greater than the spill frequency. The frequency should be above the 15 Hz spill frequency in order not to miss any beam event. However the CAMAC event rate has been found to be quite low in this early stage, around 0.20 Hz<sup>5</sup>, since only two layers of the MRD are used, in addition to the Veto. This suggest that the modules present data only the ~1.3% of the time.

Concerning the MRD DAQ, the longest portion of the chain is the CAMAC addressing and data collecting. The software has been tested using software triggering, employing the test functions of the modules, and counting the time required for 100,000 repeated cycles with 1.3% firing probability; the frequency was afterward estimated. The result is shown in Fig. 3.3, where frequency vs number of channel is plotted for TDC modules. It's clear that the frequency is well above the lower theoretical limit of 15 Hz. Rescaling the frequency to full time firing, i.e. the number of channel to be read is maximum for every DAQ cycle, the limit is easily reached with just ten modules, corresponding to five layers of MRD, Veto excluded.

For these reasons, the command stack of the CCUSB controller is not employed, because the USB connection can provide fast enough communication to address all the active cards.

<sup>5</sup>The rate is measured from output ROOT file, dividing the number of entries, i.e. events, by the time passed between the first and the last timestamp.

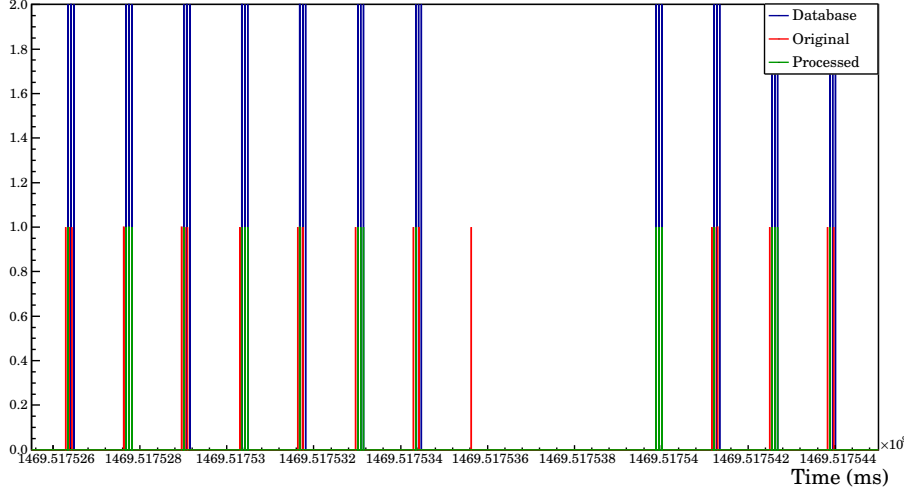


**Figure 3.4:** Detail of the time stamp alignment with the database data.

Concerning the TimeStamp, a time variable drift in the MRD TimeStamps has been found, likely due to imprecise synchronisation with the NTP server (accuracy given to be less than 30 ms) which occurs every 1024 ms. A post-processor has been written to fix the TimeStamps, identifying time patterns in the spill spectrum and comparing them to the database information. In Fig. 3.4 a detail of the result of the synchronisation is plotted. The blue lines are given by the database, used as a reference. The timestamps before and after the post-processing are printed respectively in red and green.

The post-processor also handles other aspects of the raw data, like converting the module's values into physical quantities and mapping each channel to its PMT.

### 3.3 Future improvement

Downsampling -> was it worth it? Zero suppression is cooler for memory issues, takes a lot of memory.

Integration between Chains, using timestamps now and database. This technique is ok, but the chains must be implement end better each other.

One solution could be to create a tool to govern the MRD chain, as in Fig. 3.5

The final version of the DAQ system needs a full integration of the Main Chain with the CAMAC one. A possible solution is depicted in Fig. 3.5. A new tool could be employed to embody a simplified verion of the MRD ToolChain, rather than run it in a parallel process. The MRD Chain, as proved in previous sections, is fast in execution, so it should not significantly slow down the Main DAQ. In this way, the TimeStamp synchronisation technique is not required anymore because all the acquisitions are done by the same CPU and simultaneously. As far as the output files are concerned, the ROOT trees could be merged into a single ROOT file triggering the two recording tools with ZeroMQ communication. Final reconstruction of PMTs data and MRDs could be done in a post-processing stage.

In view of the next phases of the experiment, an other DAQ-related issue is the memory storage. During early test runs, the digitiser would sample at a frequency of 500 MHz, but it has been promptly downgraded to 125 MHz because of lack of long term memory storage. As a matter of fact, noise is mostly shown in the 80  $\mu$ s time window and the meaningful signal is limited short, compared to the time window. Considering that an high time resolution is pointless in the R&D stage of the experiment, the downgrade was established. Soon, zero suppression method would be employed, which will definitely overcome storage needs. The preliminary data analysis undertaken can back this decision up, as explained in section [ref].

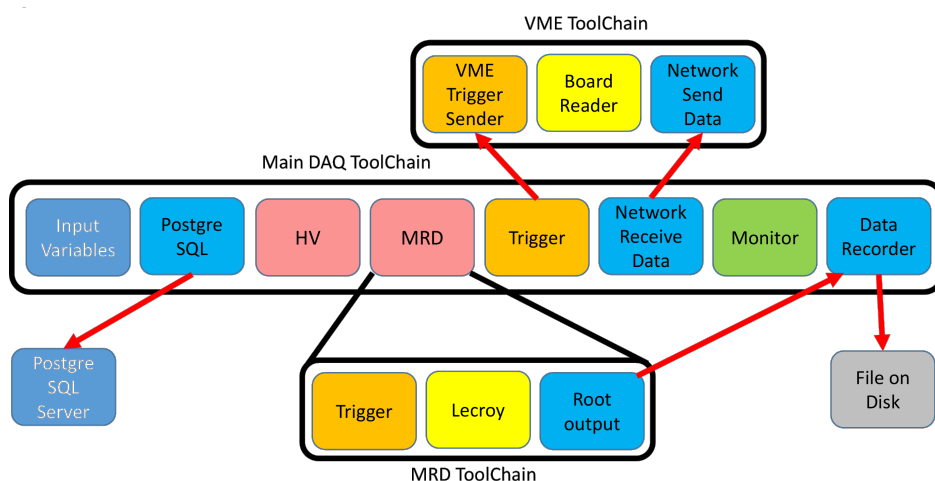


**Figure 3.5:** Final version of ANNIE's DAQ, with all the Chains integrated.

# Chapter 4

## Data Analysis procedures

This chapter deals with the data analysis techniques developed in order to study PMTs data. These methods focus on the rejection of background signals with respect to event signals which is done with individual pulse analysis. Some of these procedures could be used in future phases of the experiment, in particular the ones with LAPPDs.

Specification of runs As explained in chapter 3, the DAQ creates a new *Run* everytime it is restarted. Due to being an R&D phase, the DAQ has been improved in various occasion during data taking, hence the size and the number of files of the *Runs* are not constant. Every single file is a ROOT file containing a Tree and one of its branches holds the post-processed buffer from the digitisers. The data array is scanned by the Analysis software, entry by entry.

How measurement are made.

### 4.1 Inidivual pulse analysis

The Analysis software scans all the files which the *Run* consists of. The data array is the time profile of the PMTs outputs. [Pic of time profile] The code looks for any peak above a certain voltage threshold, defining a time window around it, of a predefined length. A length of 100 samples was chosen, resulting in a  $0.8 \mu\text{s}$  long window. The position of the peak inside this window was set to 20% of its length. This set of data is called “pulse” and it’s afterward post processed. The length and the peak position were chosen in a way that the reflection peaks are counted as one single pulse.

Every pulse is analysed by the software and some quantities are inferred from each. These values are:

**Baseline** is given by the average of first 10 points of the pulse; this value is then subtracted from the whole array.

**Height** is the height of the peak (maximum) with respect to the zero.

**Peak to valley** it is the time distance from the peak to the valley (minimum);

**Start** is position of the 25% of the rising edge of the pulse, estimated with precision using cubic interpolation<sup>1</sup>.

**Width** is the time that spans from Time to the 5% of the falling edge of the pulse, calculated using the same algorithm employed for Time.

**Charge** is the sum of the 5 points around peak, weighted by the bin width.

**Energy** is the sum of the points from Time to Time+Width, with bin weight.

**Area** is the area of the modulus of the pulse.

**Time of flight** is the time difference between Time and RWM signal.

---

<sup>1</sup>The algorithm looks for four points around the threshold which are used to define a cubic function. Using Newton’s method, the time position is found.

**Previous** is the Time of the previous pulse, if from the same PMT.

Moreover, VETO and MRD layers coincidences are recorded.

#### 4.1.1 Event definition

For every Trigger, the time distribution of the peaks is also studied, since it helps to find coincidences between PMTs. With the help of an histogram, an allowance of  $0.8 \mu\text{s}$  is given to count the coincidence magnitude of the Event and an *Event* is appointed to any cluster delimited by a bin greater than a defined threshold up to the number of PMTs fired at the same time falls to zero. [insert event picture here] In order to estimate the precise time position of the event, a weighted average is done among bins.

Improve here! What can be counted as an event? Cosmic: it would be great to calculate the expected flux in the tank. Here? Beam: the pmts will only takes a snippet from the cherenkov cone. So? Radiation: this sucks. I could estimate the number of PMTs on for each scenarios. Place some pictures here and there.

#### 4.1.2 Signal and noise discrimination

I mean event from dark noise. No dark noise run was taken (empty tank, maybe when LAPPDs will be installed). A time window is defined using the Event time position and it is used as a rejection interval. Every pulse that falls within this interval is designated as a “signal”; otherwise it is “noise”. Following this discrimination paradigm, two ROOT trees, one for signals and one for events, are filled with the pulses features, along with the pulse shape itself. In ROOT file two trees are saved, tEvent and tNoise

# Chapter 5

## Data analysis

very scarce section, for now.

For the analysis, 6 runs were selected:

Run	Description	Data size (kB)
93	beam off, trigger random	65027961
94	beam off, trigger random	41102486
120	after card synchronisation	19887893
121	after card synchronisation	6735270
145	PMT mounted on NCV	37204525
146	PMT mounted on NCV	39050909

### 5.1 Cosmic background data

With the beam off, only cosmic rays and background leave a trace in the detector. Therefore runs 93 and 94's sources are useful to characterise the background.

### 5.2 Threshold dependance

Three parameters of the Data Analysis software have been tuned so as to study the feedback of the rejection method. The parameters are:

1. Voltage threshold;
2. Number of PMTs fired;
3. Time rejection window.

#### 5.2.1 Voltage

#### 5.2.2 PMTs fired

#### 5.2.3 Rejection window

### 5.3 Michel decay

I've seen it, it could be a nice plot to place here.

### 5.4 Neutron yield

No luck yet. really not sure about this section.

## 5.5 First MRD data

TDC, could do some dummy analysis.

# Chapter 6

## Conclusions



## Appendix A

# Booster Neutrino Beam

Arxiv 1311.5958v1. Fermilab has two major neutrino beamlines: the Neutrino Main Injector (NuMI) and the Booster Neutrino Beam (BNB). The energy range of these two neutrino sources on-axis is in the GeV range, which is too high to satisfy the condition for dominance of coherent scattering. The far-off-axis ( $> 45^\circ$ ) of the BNB produces well defined neutrinos with energies below 50 MeV. The BNB source has substantial advantages over the NuMI beam source owing to suppressed kaon production from the relatively low energy 8 GeV proton beam on the target ref. Therefore, pion decay and subsequent muon decay processes are the dominant sources of neutrinos. At the far-off-axis area, the detector can be placed close enough to the target to gain a large increase in neutrino flux due to the larger solid angle acceptance.

### A.1 BNB details

An initial study using the existing BNB MC has confirmed that this approach is promising. The Fermilab Booster is a 474-meter-circumference synchrotron operating at 15 Hz. Protons from the Fermilab LINAC are injected at 400 MeV and accelerated to 8 GeV kinetic energy. The structure of the beam is a series of 81 proton bunches each with a 2 ns width and 19 ns apart. The maximum average repetition rate for proton delivery to the BNB is 5 Hz and  $5 \times 10^{12}$  protons per pulse. The repetition limit is set by the horn design and its power supply. The target is made of beryllium divided in seven cylindrical sections in a total of 71.1 cm in length and 0.51 cm in radius. In order to minimize up-stream proton interactions, the vacuum of the beam pipe extends to about 152 cm upstream of the target. The horn is an aluminum alloy toroidal electromagnet with operating values of 174 kA and maximum field value of 1.5 Tesla. A concrete collimator is located downstream of the target and guides the beam into the decay region. The air-filled cylindrical decay region extends for 45 meters. The beam stop is made of steel and concrete.

PHYSICAL REVIEW D 79, 072002 (2009). The Fermi National Accelerator Laboratory (FNAL) booster is a 474-meter-circumference synchrotron operating at 15 Hz. Protons from the Fermilab LINAC are injected at 400 MeV and accelerated to 8 GeV kinetic energy (8:89 GeV=c momentum). The booster has a harmonic number of 84, of which 81 buckets are filled. The beam is extracted into the BNB using a fast-rising kicker that extracts all of the particles in a single turn. The resulting structure is a series of 81 bunches of protons each 2 ns wide and 19 ns apart. Upon leaving the booster, the proton beam is transported through a lattice of focusing and defocusing quadrupole (FODO) and dipole magnets. A switch magnet steers the beam to the main injector or to the BNB. The BNB is also a FODO that terminates with a triplet that focuses the beam on the target. The design and measured optics of BNB are in agreement [7,8]. The maximum allowable average repetition rate for delivery of protons to the BNB is 5 Hz (with a maximum of 11 pulses in a row at 15 Hz) and  $5 \times 10^{12}$  protons-per-pulse. The 5 Hz limit is set by the design of the horn (described below) and its power supply.

The target consists of seven identical cylindrical slugs of beryllium arranged to produce a cylinder 71.1 cm long and 0.51 cm in radius. The target is contained within a beryllium sleeve 0.9 cm thick with an inner radius of 1.37 cm. Each target slug is supported within the sleeve by three “fins” (also beryllium) which extend radially out from the target to the sleeve. The volume of air within the sleeve is circulated to provide cooling for the target when the beam line is in operation. The target and associated assembly are shown in Fig. 2, where the top figure

shows an exploded view of the various components (with the downstream end of the target on the right), and the bottom shows the components in assembled form. The choice of beryllium as the target material was motivated by residual radioactivity issues in the event that the target assembly needed to be replaced, as well as energy loss considerations that allow the air-cooling system to be sufficient. Upstream of the target, the primary proton beam is monitored using four systems: two toroids measuring its intensity (protons-per-pulse), beam position monitors (BPM) and a multiwire chamber determining the beam width and position, and a resistive wall monitor (RWM) measuring both the time and intensity of the beam spills. The vacuum of the beam pipe extends to about 5 feet upstream of the target, minimizing upstream proton interactions. The toroids are continuously calibrated at 5 Hz with their absolute calibrations verified twice a year. The calibrations have shown minimal deviation ( $< 0.5\%$ ). The proton flux measured in the two toroids agree to within 2%, compatible with the expected systematic uncertainties. The BPMs are split-plate devices that measure the difference of charge induced on two plates. By measuring the change in beam position at several locations without intervening optics, the BPMs are found to be accurate to 0.1 mm (standard deviation). The multiwire is a wire chamber with 48 horizontal and 48 vertical wires and 0.5 mm pitch. The profile of the beam is measured using the secondary emission induced by the beam on the wires. The RWM is located upstream of the target to monitor the time and intensity of the proton pulses prior to striking the target. While the data from the RWM did not directly enter analysis, it allowed many useful cross checks, such as those shown in Fig. 3. The left figure shows a comparison of the production times of neutrinos observed in the MiniBooNE detector estimated based on the vertex and time reconstructed by the detector and subtracting the time-of-flight. This time is then compared to the nearest bucket as measured by the RWM. The distribution indicates that neutrino events can be matched not only to pulses from the booster, but to a specific bucket within the pulse. The tails of the distribution result from the resolution of the vertex reconstruction of the neutrino event in the detector, which is needed to determine the time of the event and correct for the time-of-flight. The right plot demonstrates the synchronization of the horn pulse (described in Sec. II C) with the delivery of the beam as measured by the RWM.

The horn current pulse is approximately a half-sinusoid of amplitude 174 kA, 143 s long, synchronized to each beam spill.

The typical beam alignment and divergence measured by the beam position monitors located near the target are within 1 mm and 1 mrad of the nominal target center and axis direction, respectively; the typical beam focusing on target measured by beam profile monitors is of the order of 1–2 mm [root mean square(RMS)] in both the horizontal and vertical directions. These parameters are well within the experiment requirements. The number of protons delivered to the BNB target is measured for each proton batch using two toroids located near the target along the beam line. The toroid calibration, performed on a pulse-by-pulse basis, provides a measurement of the number of protons to BNB with a 2% accuracy. Primary protons from the 8 GeV beam line strike a thick beryllium target located in the BNB target hall.

The SciBooNE hall is on axis from the Booster Neutrino Beam (BNB) at 8 m below the surface. The BNB impinges 8.89 GeV/c protons from the booster on a beryllium target, with 4 x10to12 delivered in a narrow spill of approximately 1.6 micros at a frequency of 7.5 Hz. The projected number of protons incident on the target (POT) per year for the BNB is about 2 x 10to 20 POT. The rates expected per year when running in neutrino mode for 1 ton of water (the approximate usable fiducial volume) are about 16K neutrino interactions, where 11K of those would be numu CC interactions. This spectrum peaks ideally in the region of interest at 700 MeV as shown left of Figure 2 and has the target rate of neutrino interactions per year. The spectrum and rates are based on BNB flux simulated data provided by Zarko Pavlovic (FNAL)appropriately propagated to the SciBoone hall.

The target is made of seven cylindrical slugs for a total target length of 71.1 cm, or about 1.7 inelastic interaction lengths. The beryllium target is surrounded by a magnetic focusing horn, bending and sign-selecting the secondary particles that emerge from the interactions in the target along the direction pointing to the SciBooNE detector. The focusing is produced by the toroidal magnetic field present in the air volume between the horn's two coaxial conductors made of aluminum alloy. The horn current pulse is approximately a half-sinusoid of amplitude 174 kA, 143 s long, synchronized to each beam spill. The polarity of the horn current flow can be (and has been) switched, in order to focus negatively charged mesons, and therefore produce an antineutrino instead of a neutrino beam. The beam of focused, secondary mesons emerging from the

target/horn region is further collimated, via passive shielding, and allowed to decay into neutrinos in a cylindrical decay region filled with air at atmospheric pressure, 50 m long and 90 cm in radius. A beam absorber located at the end of the decay region stops the hadronic and muonic component of the beam, and only a pure neutrino beam pointing toward the detector remains, mostly from a pion to mu<sup>+</sup> nuofmu decays.

## A.2 Resistive Wall Monitor

A resistive wall monitor measures the image charge that flows along the vacuum chamber following the beam. The image charge has equal magnitude but opposite sign. Depending on the beam velocity, the image charge will lag behind and be spread out along its path. The ultimate bandwidth of such a detector is limited by this spreading of the electric field lines between the beam and the inside walls of the beam pipe. The spreading angle is approximately  $1/\gamma$  for relativistic beams ( $\gamma$  is the ratio of total energy to rest energy). The estimated bandwidth limit from spreading is 47 GHz at injection to the Main Injector for a 3 cm radius pipe and 8 GeV proton energy. In practice, the detector response is difficult to maintain above the microwave cutoff frequency of the beam pipe, measured to be 1.5 GHz for the elliptical beam pipe used in the Main Injector. Above cutoff, the characteristic impedance of the beam pipe and the impedance of nearby structures such as bellows or changes in geometry can effect accuracy.

In order to measure the image current, the beam pipe is cut and a resistive gap is inserted (Figure 1). Various ferrite cores are used to force the image current through the resistive gap rather than allowing it to flow through other conducting paths. In addition to image current, other currents are often found flowing along the beam pipe. The gap and cores are placed inside a metal can to shunt these “noise” currents around rather than through the resistive gap. The inductance of the cores and the resistance of the gap forms a high pass filter with a corner frequency of  $R/2\pi L$ , typically a few kilohertz. Above this frequency, cores act to minimize the net current through their center by inducing a current through the resistive gap that just cancels the beam current. The gap impedance is chosen to be well below the impedance of the cores inside the shielding can. Several types of ferrite and microwave absorbers are used to maximize the impedance and minimize resonances within the desired bandwidth. The Main Injector shielding can has an impedance greater than 30 ohms with the ferrite cores. In parallel with the 1 ohm gap impedance, 30 ohms can cause frequency dependent errors of pm1.5% or 0.15 db. If the charge density around the circumference of the gap is not uniform, the voltage across the gap will vary around the circumference. The gap will act as an azimuthal transmission line transporting charge until the voltage equalizes. The time domain response of the detector would be distorted during this time. Position detectors have been made by exploiting this effect. The elliptical shape of the Main Injector pipe aggravates this problem (Figure 2). To overcome this problem, a round geometry is used for the gap and the signals from several monitor points equally spaced around the circumference are combined to form a single output.



# Appendix B

## Employed CAMAC modules

B.1 USB Camac Controller

B.2 TDC

B.3 ADC

